Significant improvement of optical traps by tuning standard water immersion objectives

Significant improvement of optical traps by tuning standard water immersion objectives

S Nader S Reihani[1,2]**, Shahid A Mir**[1]**, Andrew C Richardson**[1] **and Lene B Oddershede**[1]

[1] The Niels Bohr Institute (NBI), Copenhagen University, DK-2100Ø, Copenhagen, Denmark
[2] Department of Physics, Institute for Advanced Studies in Basic Sciences (IASBS), Gava Zang, PO Box 45195-1159, Zanjan 45137-66731, Iran

E-mail: oddershede@nbi.dk

Abstract
Focused infrared lasers are widely used for micromanipulation and visualization of biological specimens. An inherent practical problem is that off-the-shelf commercial microscope objectives are designed for use with visible and not infrared wavelengths. Less aberration is introduced by water immersion objectives than by oil immersion ones, however, even water immersion objectives induce significant aberration. We present a simple method to reduce the spherical aberration induced by water immersion objectives, namely by tuning the correction collar of the objective to a value that is ∼10% lower than the physical thickness of the coverslip. This results in marked improvements in optical trapping strengths of up to 100% laterally and 600% axially from a standard microscope objective designed for use in the visible range. The results are generally valid for any water immersion objective with any numerical aperture.

Keywords: optical trapping, water immersion objective, aberration, trap efficiency, infrared laser

(Some figures in this article are in colour only in the electronic version)

1. Introduction

A laser beam focused to a diffraction limited spot is used for a variety of applications in biophysics, the life sciences, and nanotechnology. For instance, focused lasers are used for confocal visualization of biological specimens, nano-fabrication, and nano-surgery. Also, strongly focused laser beams are used for optical trapping of dielectric particles with sizes down to nanometers [1–3] and very successfully for quantitative investigations of biological polymers and their associated molecular motors [4, 5]. For such applications, it is crucial that the light is tightly focused and that essentially no power is lost outside the region of interest. The size of the focal spot directly depends on the numerical aperture (NA) of the objective—the larger the NA the smaller the spot size. The NA is defined by the largest angle at which the light rays are collected by the objective. Oil immersion objectives provide the highest NA (NA up to 1.65 is commercially available); however, for typical use within an optical trap, the total internal reflection at the interface between chamber and sample (glass/water) limits the practical NA to 1.33. Spherical aberration (SA) arises, e.g., due to refractive index mismatch between the immersion and specimen media, and causes a broadening of the spot size as the focus is moved into the sample. This limits the functionality of oil immersion objectives for in-depth applications. Although water immersion objectives have lower NA (NA up to 1.2 is commercially available), they are generally preferred for in-depth trapping inside aqueous media because there is no refractive index mismatch between the immersion and sample media. Also, in contrast to oil immersion objectives, the possible aberration introduced by water immersion objectives is constant throughout the sample.

Water immersion objectives are typically optimized to focus visible light almost without introducing spherical aberration. However, in focusing of, e.g., infrared light even water immersion objectives introduce considerable SA. This can be explained by the following general argument. If a laser beam is focused into a homogeneous medium and if the objective is corrected for this there would be no spherical aberration, hence, the focal spot would be minimized. If a slab of medium with different refractive index is placed between the objective and the focus, spherical aberration arises and the focal spot broadens. This happens because different rays travel different distances inside the added medium thus gaining different phases. The gained phase depends both on the traveled distance and on the refractive index of the added medium (it is wavelength dependent). Hence, for any given objective just changing the wavelength will introduce spherical aberration. The amount of spherical aberration depends on the wavelength difference. For an infrared laser (almost double the mid-visible wavelength), there will be a considerable amount of spherical aberration weakening the trap by broadening the focal spot. As infrared lasers are less harmful to biological specimens than lasers emitting visible light, most optical traps for bio-specimen investigations use infrared lasers and hence suffer from SA.

SA appears as a phase in the pupil function and can be balanced by introducing SA from different sources. In practice this can be accomplished, e.g., by changing tube length of the focusing system [6, 7], by changing the index of refraction of the immersion medium [8], or by a combination of the two [9]. If a spatial light modulator (SLM) is available, there also exists an elegant method of performing an *in situ* wavefront correction in order to minimize the spherical aberration [10]. Here we show that the SA introduced when a standard water immersion objective is used to focus infrared light can be efficiently reduced simply by altering the value of the correction collar (CC). This gives rise to a significant improvement of up to 600% in the axial stiffness of an optical trap, the axial direction being the limiting direction for three-dimensional optical trapping. We provide a simple practical method for precise measurement of the physical coverslip thickness and a calculation of this valid for any NA and within any medium.

2. Methods

Our optical trap (OT) was based on an infrared laser beam (1064 nm, Nd:YVO$_4$, Spectra Physics BL106C) implemented in an inverted microscope (Leica, DMIRBE), see figure 1(a) for a sketch of the setup. The laser was expanded so that it slightly overfilled the back aperture of the water immersion objective (NA $= 1.2, 63\times$, Leica) by which it was focused into the chamber. The laser power was kept constant, 200 mW, at the exit of the laser, ~40 mW at the sample, throughout the measurements. A tunable CC on the body of the objective (see zoomed region in figure 1(a)) permits adjustment of an interior airspace so that coverslips of different thicknesses may be used, ranging from 0.12–0.2 mm. However, as shown here, a CC value corresponding to the actual thickness of the

coverslip is not an optimal setting for focusing of infrared light and the setting of the CC value can be tuned to significantly improve the focusing of infrared laser light. We performed a series of trapping experiments using coverslips with different thicknesses. Using a precise mechanical ruler with 1 μm resolution we measured thousands of cover glasses of types #1, #1.5, and #2, each number denoting an interval with a midpoint around which the cover glass thicknesses distribute evenly. For types #1, #1.5, and #2 the intervals are 130–160 μm, 160–190 μm, and 190–220 μm, respectively. We did not use types #0.5 (100–130 μm) or #2.5 (220–250 μm) because #0.5 was very fragile and hard to handle and #2.5 was thicker than the working distance of the water immersion objective. The goal was to find five groups of five identical cover glasses. The thicknesses of the these five groups were 144, 157, 176, 197, and 219 μm, with a precision of ± 1 μm. Twenty five perfusion chambers (five for each group) were made by separating a coverslip from a microscope slide by two strips of double sided Scotch Tape. An aqueous solution of diluted polystyrene beads with mean diameter of 0.8 μm, Bangs Laboratories, was flushed into the chambers and the chamber was sealed by vacuum grease and mounted with the coverslip facing toward the microscope objective.

An optical trap exerts a harmonic force on a trapped particle; in one dimension the force is given by $F = -\kappa_x x$, where x is the deviation from the equilibrium position and κ_x is the spring constant in the x direction. In general, the spring constant is different in each translational direction and weakest in the direction along the propagating laser light, the axial direction. In addition, the bead is subject to a frictional force, $-\gamma \dot{x}$. If far from any surface the frictional coefficient, γ, can be found through Stokes law: $\gamma = 3\pi \eta d$ where η is the viscosity of the medium and d the diameter of the bead. Finally, a stochastic force $\mathcal{F}(T, t)$ is acting on the bead which is dependent both on temperature, T, and time, t. As the Reynolds numbers are very low, the inertial term is significantly smaller than any of the external forces acting on the bead; hence, the motion of the bead in the x-direction is well described by the Langevin equation: $\gamma \dot{x} + \kappa_x x = \mathcal{F}(T, t)$. Assuming that $\mathcal{F}(T, t)$ is correctly described as ideal white noise the equation of motion can be Fourier transformed, thus yielding a Lorentzian power spectrum: $S_x(f) = \frac{k_B T}{\gamma \pi^2 (f_c^2 + f^2)}$ [11, 12]. $f_c = \frac{\kappa_x}{2\pi \gamma}$ is denoted as the corner frequency and marks the point in the power spectrum where the change occurs between the low frequencies where the bead strongly feels the confinement by the optical trapping potential and the high frequencies where the bead performs Brownian fluctuations. An example of a power spectrum is shown in figure 1(b). During the calibration procedure a Lorentzian function is fitted to the power spectrum while taking into account the filtering effect of the photodiodes [13, 14]; the Lorentzian fit to the power spectrum is shown as a full line in figure 1(b). The viscosity, η, of the medium (water) was 0.001 Pa s and the temperature was 298 K. The temperature increase due to absorption of the incident laser light of a micron-sized polystyrene particle at these laser powers is below 1 K [15, 16].

The diameter of the beads, 0.8 μm, was chosen so that the trapping strength became equal in both lateral directions [17].
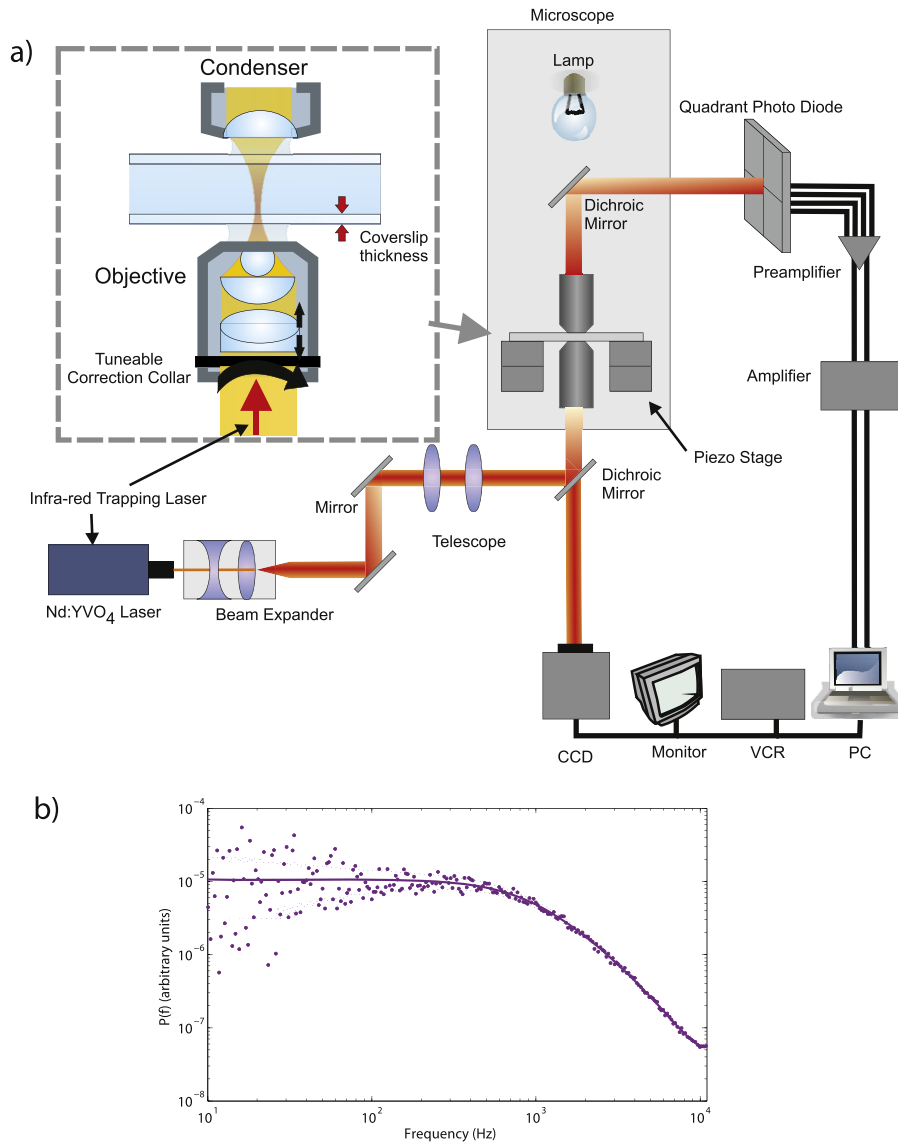
Figure 1. (a) Sketch of the setup. The optical trap based on an Nd:YVO$_4$ laser is implemented in an inverted microscope (gray region). The dashed box shows a zoom-in on the water immersion objective, the sample, and the condenser; the tunable correction collar is located at the lower edge of the objective. (b) Typical power spectrum of the lateral thermal fluctuations of an optically trapped polystyrene bead in an experiment with cover glass thickness 178 μm and the collar value set to 160 μm.

Within each chamber, a bead was trapped and moved to a constant depth of 5 μm where its positional time series was recorded using a quadrant photodiode (Hamamatsu Si-PIN S5981) operating at a sampling rate of 22 kHz. For each sample chamber five positional time series were recorded and analyzed.

3. Results

Varying the CC setting has huge implications for the optical trapping strength. This is shown in figure 2, where the upper graph (a) shows the spring constant in the lateral direction and the lower graph (b) shows the spring constant in the axial direction. As the two lateral directions within the uncertainties yielded similar spring constants only x is shown. Figure 2 shows the following. (1) Tuning the CC to a value equal to the

real physical thickness, d_R, does not provide the strongest trap; for coverslips with $d_R = 144$ μm, the strongest trap, and thus the lowest aberration occurs for a CC setting of $\sim$126 μm. We denote the optimal CC setting by d_{opt}. (2) The trap produced by setting CC to d_{opt} is significantly stronger than if the CC value is set to d_R. In the axial direction the discrepancy between the optimal CC setting and the physical real thickness of the coverslip is larger than for the lateral directions. We found improvements of trapping efficiencies of up to 100% in lateral and 600% in axial stiffnesses by using a CC value equal to d_{opt} instead of using the CC value suggested by the microscope manufacturer. Hence, this method significantly sharpens the intensity distribution by reducing the SA, in particular in the axial direction.

We found the CC value corresponding to the least amount of spherical aberration (the strongest optical trap) by
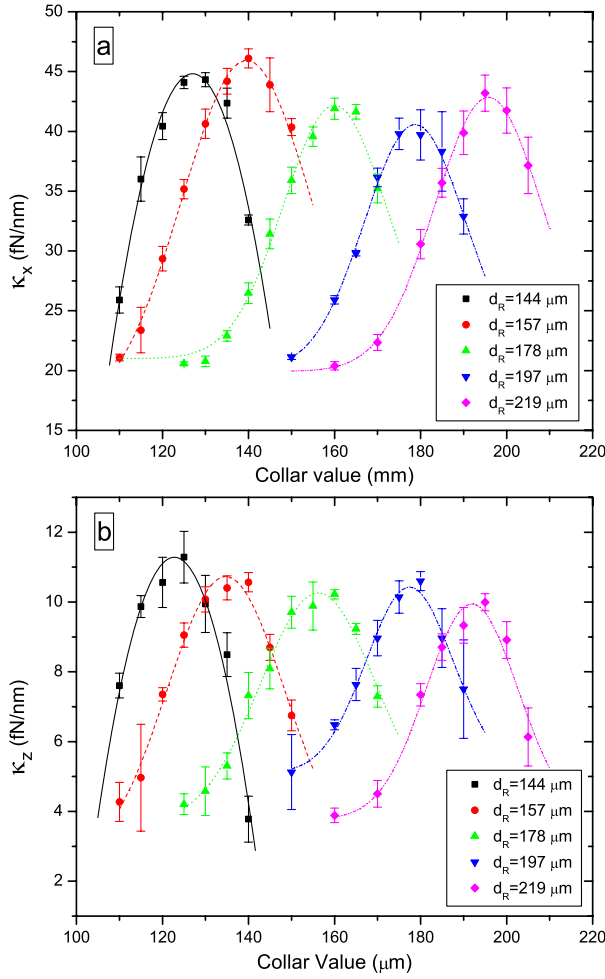
Figure 2. The stiffness of an optical trap in the lateral (a) and axial (b) directions for coverslips with physical thicknesses of 144 (black squares), 157 (red circles), 176 (green triangles), 197 (blue upside down triangles), and 219 μm (magenta diamonds). The curves show Gaussian fits to each data set.

performing a Gaussian fit to each of the data sets presented in figure 2; d_{opt} is chosen as the CC value corresponding to the peak of the Gaussian function. Figure 3 shows a comparison of d_{opt} to the real physical thickness of the coverslip, d_R. More precisely, the relative difference, $\delta = (d_R - d_{opt})/d_R$, is depicted as a function of d_R. δ varies slightly with coverslip thickness; however, for all coverslip thicknesses the relative differences are fairly close to the average values (horizontal lines in figure 3). In other words, tuning the CC to a value which is smaller than the real thickness by $\sim$10.5% (or $\sim$12.7%) one can get improvements as high as $\sim$100% (or $\sim$600%) in the lateral (or axial) trapping stiffness. These careful and precise measurements were all made using the Leica objective mentioned in section 2. Furthermore, we tested the idea on optical traps formed by an Olympus objective (UPLSAPO 60$\times$ W, NA = 1.2) and by a Zeiss objective (Apochromat 63$\times$ W, NA = 1.2). Tuning the CC values of the Olympus and Zeiss water immersion objectives indeed had an effect on the strength of the optical trap similar to tuning the CC value of the Leica objective. When the CC value was tuned to a value approximately 10% lower than the real thickness,
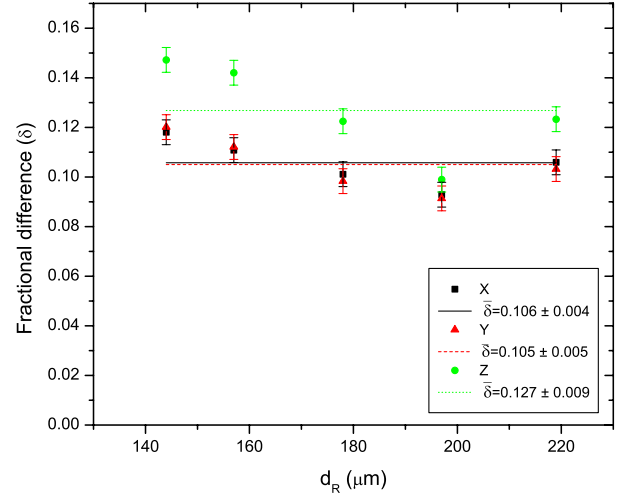
Figure 3. The relative difference between the optimal CC value and the real physical thickness of the coverslip for the *X* (black squares), *Y* (red diamonds), and *Z* (green circles) directions. Horizontal lines denote the average values. Error bars are one standard deviation.

improvements in axial trapping strength of several hundred per cent were seen.

To implement this method the user needs to know d_R for the particular coverslip used. The thickness given by the manufacturer serves as a guide to this value, but a more trustworthy method is to perform an actual measurement. It is not always practical to mechanically measure the coverslip thickness before mounting it in the chamber. Fortunately, the measurement can also be done on a mounted coverslip by using the trapping laser: there is a refractive index contrast between the glass and the water at the two surfaces of the coverslip; hence, when the laser focus is moved through the sample by moving the objective, two objective positions exist where the reflected laser light appears to have the smallest diffraction pattern. These positions indicate the two surfaces of the coverslip. The distance traveled by the objective between these two consecutive reflections is denoted by d_{obj} and can be measured. However, due to the focus shift, the value of d_{obj} is not identical to d_R [18]. Figure 4(b) (black squares) shows the relation between d_{obj} and d_R for the five different coverslip sizes. The values of d_{obj} are consistently lower than the corresponding values of d_R; they appear linearly related with a slope of 0.82 ± 0.02.

Instead of performing a cumbersome mechanical measurement of the real thickness of each coverslip, the real thickness, d_R, can be calculated from the observed value of d_{obj} for any water immersion objective with any NA and in any medium. Figure 4(a) shows the optical pathway for marginal rays and for geometrical reasons it follows that

$$\frac{d_R}{d_{obj}} = \frac{\tan\theta_1}{\tan\theta_2} = \frac{n_2}{n_1}\sqrt{1 + \tan^2\theta_1\left[1 - \left(\frac{n_1}{n_2}\right)^2\right]}, \quad (1)$$

where n_1 and n_2 represent the refractive indices of water and glass, respectively. For normal lenses for which the principal plane is flat, the radial distance of the rays from the optical axis
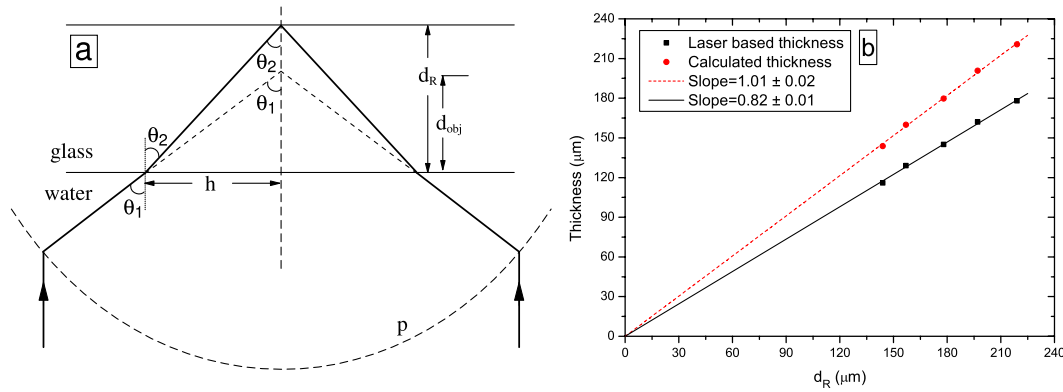
Figure 4. (a) Sketch of the optical path for marginal rays traveling from water to glass. (b) Relation between the reflection based thickness measurement, d_{obj}, and the real thickness, d_{R}, of coverslips (black squares); the slope of the linear fit is 0.82 ± 0.02 (black full line). Also shown is the relation between the calculated and real values of d_{R} (red circles); the slope of the linear fit is 1.01 ± 0.03 (red dashed line).

scales with $\tan \theta$. However, for normal objectives satisfying Abbe's sine condition the principal plane is hemispherical. In the latter case the lateral distance of a given ray from the optical axis scales with $\sin \theta$. To account for this correction $\tan \theta$ should be replaced by $\sin \theta = \frac{\text{NA}}{n_1}$ in equation (1), thus yielding the final result:

$$\frac{d_{\text{R}}}{d_{\text{obj}}} = \frac{n_2}{n_1} \sqrt{1 + \left(\frac{\text{NA}}{n_1}\right)^2 \left[1 - \left(\frac{n_1}{n_2}\right)^2\right]}. \qquad (2)$$

In our experiments, NA = 1.2, $n_1 = 1.33$, and $n_2 = 1.518$ thus yielding $\frac{d_{\text{R}}}{d_{\text{obj}}} = 1.24$. Using this relation we calculated d_{R} from the measured values of d_{obj}; the result is shown in figure 4(b) (red circles). As the calculated values of d_{R} and the real measured thickness are directly linearly correlated with a slope of 1.01 we find that equation (2) correctly finds the real coverslip thickness from the measured value of d_{obj}.

4. Conclusion

Water immersion objectives are optimized to minimize the spherical aberration in the visible region. However, an infrared optical trap becomes significantly aberrated when focused by such an objective. We have systematically shown that by simply tuning the value of the correction collar of the objective to a value 10–13% lower than the physical thickness of the coverslip, the performance of the optical trap can be improved by 100% in the lateral and 600% in the axial directions. This result is important not only for optical trapping but for any application requiring a tight focusing of infrared light using a standard microscope objective designed for visible wavelengths.

If infrared optical trapping is combined with fluorescent microscopy [19] utilizing visible wavelengths there is a potential conflict of whether the signal from the fluorophores or the efficiency of the optical trap should be optimized as a given condition with inherent spherical aberration will at most optimize either in the infrared or in the visible. However, experience with simultaneous infrared optical trapping and visualization at lower wavelengths of individual quantum

dots [20] or metallic nanoparticles [16, 21] which are challenging both to trap and to visualize shows that an infrared optical trap is more susceptible to spherical aberration than visualization in the visible range. Hence, for combined infrared optical trapping and visible fluorescent assays of challenging objects is it advisable to compensate aberrations in the infrared.

References

[1] Ashkin A, Dziedzic J M, Bjorkholm J E and Chu S 1986 Observation of a single-beam gradient force optical trap fordielectric particles *Opt. Lett.* **11** 288–90

[2] Bosanac L, Aabo T, Bendix P M and Oddershede L B 2008 Efficient optical trapping and visualization of silver nanoparticles *Nano Lett.* **8** 1486–91

[3] Hajizadeh F and Reihani S N S 2010 Optimized optical trapping of gold nanoparticles *Opt. Express* **18** 551–9

[4] Bustamante C, Bryant Z and Smith S B 2003 Ten years of tension: single-molecule DNA mechanics *Nature* **421** 423–7

[5] Greenleaf W J, Woodside M T and Block S M 2007 High-Resolution, single-molecule measurements of biomolecular motion *Annu. Rev. Biophys. Biomol. Struct.* **36** 171–90

[6] Reihani S N S, Khalesifard H R and Golestanian R 2006 Measuring lateral efficiency of optical traps: the effect of tube length *Opt. Commun.* **259** 204–11

[7] Reihani S N S, Charsooghi M A, Khalisifard H R and Golestanian R 2006 Efficient in-depth trapping with an oil-immersion objective lens *Opt. Lett.* **31** 766–8

[8] Reihani S N S and Oddershede L B 2007 Optimizing immersion media refractive index improves optical trapping by compensating spherical aberrations *Opt. Lett.* **32** 1998–2000

[9] Reihani S N S and Oddershede L B 2009 Confocal microscopy of thick specimens *J. Biomed. Opt.* **14** 030513

[10] Cizmar T, Mazilu M and Dholakia K 2010 *In situ* wavefront correction and its application to micromanipulation *Nature Photon.* **4** 388–94

[11] Gittes F and Schmidt C F 1998 Signals and noise in micromechanical measurements *Methods Cell Biol.* **55** 129–56

[12] Berg-Sørensen K and Flyvbjerg H 2004 Power spectrum analysis for optical tweezers *Rev. Sci. Instrum.* **75** 594–612

[13] Berg-Sørensen K, Oddershede L, Florin E L and Flyvbjerg H 2003 Unintended filtering in typical photo-diode detection system for optical tweezers *J. Appl. Phys.* **93** 3167–76

[14] Hansen P M, Tolic-Nørrelykke I M, Flyvbjerg H and
     Berg-Sørensen K 2006 Tweezercalib 2.0: Faster version of a
     MatLab package forprecision calibration of optical tweezers
     Comput. Phys. Commun. **174,** 518–20

[15] Peterman E J G, Gittes F and Schmidt C F 2003 Laser-induced
     heating in optical traps *Biophys. J.* **84** 1308–16

[16] Bendix P M, Reihani S N S and Oddershede L B 2010 Direct
     measurements of heating by electromagnetically trapped
     gold nanoparticles on supported lipid bilayers *ACS Nano*
     4 2256–62

[17] Rohrbach A 2005 Stiffness of optical traps: quantitative
     agreement between experiment and electromagnetic theory
     Phys. Rev. Lett. **95** 168102

[18] Neuman K C and Block S M 2004 Optical trapping *Rev. Sci.
     Instrum.* **75** 2787–809

[19] Lee W M, Reece P J, Marchington R F, Metzger N K and
     Dholakia K 2007 Construction and calibration of an optical
     trap on a fluorescence optical microscope *Nature Protocols*
     2 3226–38

[20] Jauffred L, Richardson A C and Oddershede L B 2008
     Three-dimensional optical control of individual quantum
     dots *Nano Lett.* **8** 3376–80

[21] Kyrsting A, Bendix P M, Stamou D G and Oddershede L B
     2011 Heat profiling of three-dimensionally optically trapped
     gold nanoparticles using vesicle cargo release *Nano Lett.*
     11 888–92